Cosmological N-Body simulations

Technique, scope & limitations

Jayanti Prasad

Inter-University Centre for Astronomy & Astrophysics
Pune, India (411007)

January 13, 2011

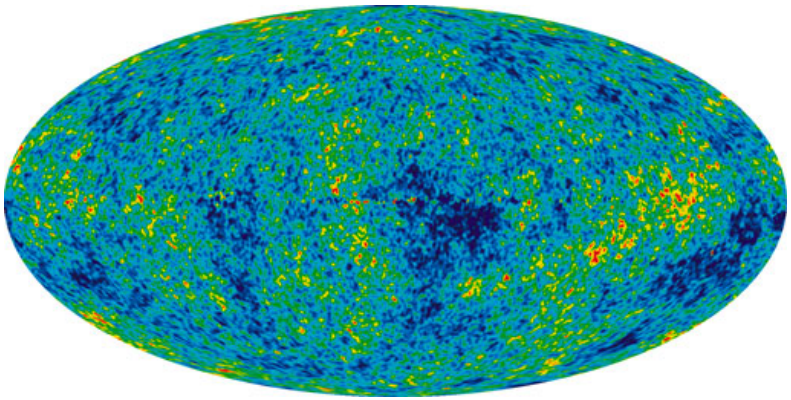

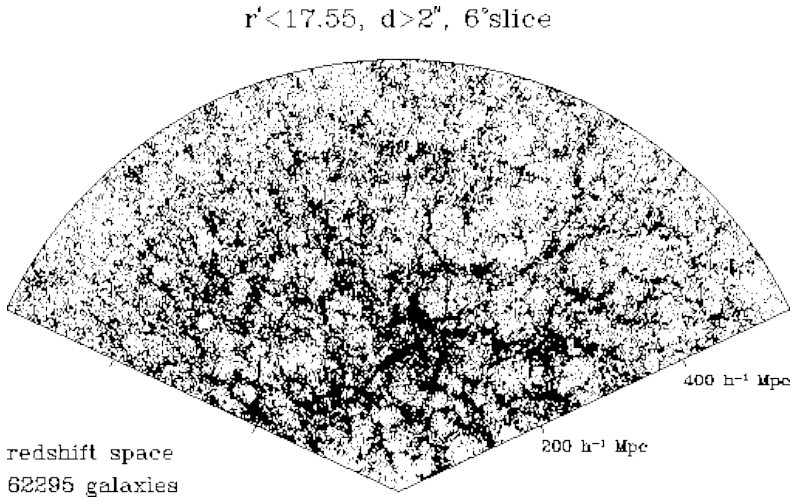
r'<17.55, d>2", 6°slice
400 h⁻¹ Mpc
200 h⁻¹ Mpc
redshift space
62295 galaxies

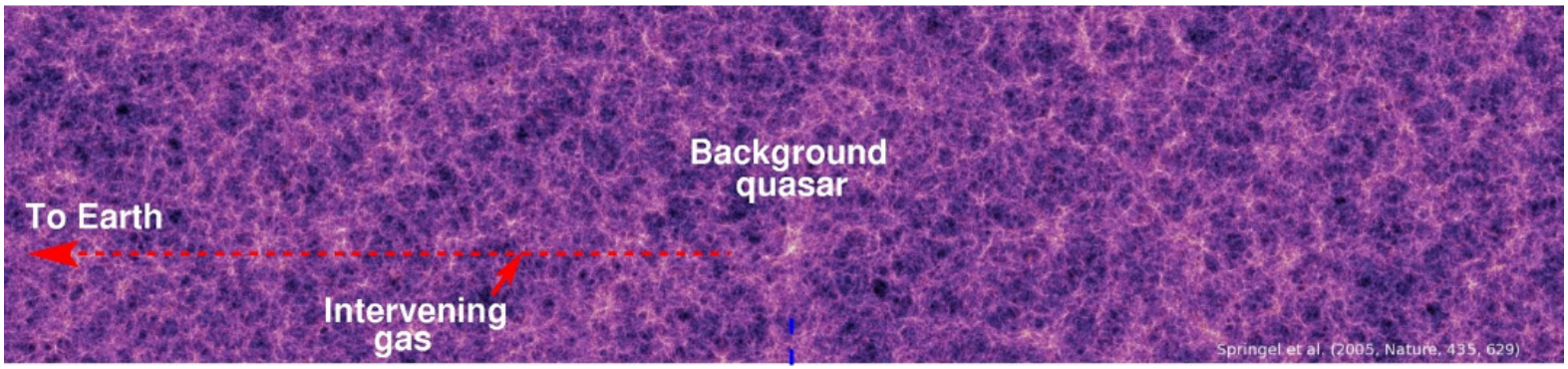
Background quasar
To Earth
Intervening gas
Springel et al. (2005, Nature, 435, 629)

Plan of the Talk

- Non-linear gravitational clustering
- Cosmological N-body simulations
- Role of substructure in gravitaional clustering
- Finite volume effects in N-body simulations
- Summary & Conclusions

Growth of perturbations

Density field

$$\delta(\mathbf{x},t)=\frac{\rho(\mathbf{x},t)-\rho_b(t)}{\rho_b(t)}=\frac{1}{a^3(t)}\sum_{i=1}^{N}m_i\delta_D(\mathbf{x}-\mathbf{x}_i(t)) \qquad (1)$$

and

$$\delta_{\mathbf{k}}(t)=\frac{1}{M}\sum_{i=1}^{N}m_i\exp(-i\mathbf{k}.\mathbf{x}_i)-\delta_D^3(\mathbf{k});\quad \text{where}\quad M=\sum_{i=1}^{N}m_i \qquad (2)$$

$$\ddot{\delta}_{\mathbf{k}}+2\frac{\dot{a}}{a}\delta_{\mathbf{k}}=\frac{1}{M}\sum_{i=1}^{N}m_i\left[-i\mathbf{k}.\left(\ddot{\mathbf{x}}_i+2\frac{\ddot{a}}{a}\dot{\mathbf{x}}_i\right)-(\mathbf{k}.\mathbf{x}_i)^2\right]\exp(-i\mathbf{k}.\mathbf{x}_i)$$

[Peebles, P. J. E. (1980)]

Dynamics of particles

$$\ddot{\mathbf{x}}_i + 2\frac{\dot{a}}{a}\dot{\mathbf{x}}_i = -\frac{\nabla_x \phi(x,t)}{a^2(t)} \tag{3}$$

$$\nabla_x^2 \phi(\mathbf{x}_i, t) = 4\pi G a^2(t) \rho_b(t) \delta(\mathbf{x}_i, t) \tag{4}$$

$$H^2(t) = H^2(t_0)\left[\frac{\Omega_m}{a^3(t)} + \Omega_\Lambda + \frac{1-\Omega_m-\Omega_\Lambda}{a^2(t)}\right] \tag{5}$$

where:

$$H(t) = \frac{1}{a(t)}\frac{da(t)}{dt}; \quad \Omega_X = \frac{8\pi G \rho_X}{3H^2(t)} \tag{6}$$

Mode Coupling

$$\ddot{\delta}_{\mathbf{k}} + 2\frac{\dot{a}}{a}\dot{\delta}_{\mathbf{k}}(t) = 4\pi G\rho_b\delta_{\mathbf{k}} + A_{\mathbf{k}} - B_{\mathbf{k}} \tag{7}$$

where

$$A_{\mathbf{k}} = 2\pi G\rho_b \sum_{\mathbf{k}'\neq 0, \mathbf{k}\neq\mathbf{k}'} \left[\frac{\mathbf{k}'.\mathbf{k}}{|\mathbf{k}'|^2} + \frac{\mathbf{k}.(\mathbf{k}-\mathbf{k}')}{|\mathbf{k}-\mathbf{k}'|^2}\right] \delta_{\mathbf{k}'}\delta_{\mathbf{k}-\mathbf{k}'} \tag{8}$$

and

$$B_{\mathbf{k}} = \frac{1}{M}\sum_{i=1}^{N} m_i(\mathbf{k}.\dot{\mathbf{x}}_i)^2 \exp(-i\mathbf{k}.\mathbf{x}_i) \tag{9}$$

[Padmanabhan (1993)]

Cosmological N-body simulations

Mass dicreatization

$$m_p = \frac{(L_{lbox}/Mpc)^3}{N_p} 2.78 \times 10^{11} M_\odot \Omega_m h^2 \tag{10}$$

Periodic boundary conditions

$$x + L_{box} \longrightarrow x \tag{11}$$

Force softening

$$\vec{F}_{ij} = -\frac{G M_i M_j \hat{r}_{ij}}{r_{ij}^2 + \epsilon^2} \tag{12}$$

[Hockney & Eastwood (1981); Efstathiou et al. (1985); Sellwood (1987); Bertschinger (1998); Aarseth (2003)]

A. Setting-up initial conditions

- The real and imaginary parts of the gravitational potential in Fourier space are drawn from a Gaussian random distribution with zero mean $P_\phi(k)$ variance

$$P(\phi_k) = \frac{1}{\sqrt{2\pi P_\phi(k)}} \exp\left[-\frac{1}{2}\frac{\phi_k^2}{P_\phi(k)}\right] \tag{13}$$

or

$$\phi_k = \text{Gauss}(0.0, P_\phi(k)) \tag{14}$$

- Initial position/velocity of particles are computed using Zelodovich Approximation

$$v = -\nabla\phi_{int} \tag{15}$$

- Normalization of $P(k)$ is given in the form of the scale of non-linearity at the final epoch and the initial epoch is computed on the basis of the maximum displacement in the first step.

B. Force computation

Particle-Particle (PP)

Direct pair-force computationally expensive i.e., $\mathcal{O}(N_p^2)$, however, accurate at all scales.

Particle-Mesh (PM)

- Force is computed by solving Poisson's equation in Fourier space (on a grid) by using Fast-Fourier-Techniques (FFT). Computational cost grows as $\mathcal{O}(N_p \log N_p)$ and force is inaccurate at sub-grid scales.
- Periodic boundary conditions and force softening are automatically incorporated.

[Efstathiou et al. (1985); Bagla & Padmanabhan (1997)].

Force..

Tree

- Tree structured hierarchical division of space into cubic cells, each of which is recursively divided into eight sub-cells whenever more than on particles are in the same cell. The tree is constructed at every time step.
- The force acting on a particle "p" due to all the particles in a cell of size l at distance d is approximated by the force acting between the particle and the "cell" if $l/d < \theta$, where θ is a parameter.

[Barnes & Hut (1986)]

TreePM

- Force is split into two parts: long range and the short range.
- Long range force is computed using PM method and the short range force is computed using Tree method.

[Bagla (2002); Bagla & Ray (2003)]

C. Moving Particles

Time centered leap-from scheme

$$x_n = x_{n-1} + v_{n-1/2}\Delta t \tag{16}$$

$$v_{n+1/2} = v_{n-1/2} + a_n \Delta t \tag{17}$$

Power spectrum and two point correlation functions

The two point correlation function $\xi(r)$ and density contrast $\delta(\mathbf{x})$ are related as

$$\xi(r) = \langle \delta(\mathbf{x}+\mathbf{r})\delta(\mathbf{x}) \rangle \tag{18}$$

Here averaging is done over an ensemble of large spatial regions of the universe that are statistically independent from each other. If we write density contrasts $\delta(\mathbf{x}+\mathbf{r})$ and $\delta(\mathbf{x})$ in terms of Fourier components and simplify equation (18) we get

$$\xi(r) = \int \frac{d^3\mathbf{k}}{(2\pi)^3} P(k) \exp(i\mathbf{k}.\mathbf{r}) \tag{19}$$

Here $P(k)$ is called the power spectrum and is defined as

$$\langle \delta_{\mathbf{k}} \delta^{\star}_{\mathbf{k}'} \rangle = (2\pi)^3 \delta_D^{(3)}(\mathbf{k}-\mathbf{k}') P(k) \tag{20}$$

Mass variance

Variance of the mass inside cells of various sizes, after smoothing the density by a window function W.

$$\sigma^2(r) = \frac{\left\langle (M - < M >)^2 \right\rangle}{< M >^2} = \frac{1}{2\pi^2} \int dk k^2 P(k) |W(k, r)|^2 \qquad (21)$$

where $M = 4\pi\rho r^3/3$. For a spherical-top hat window $W(k, r)$ is given by

$$W(k, r) = 3 \left(\frac{\sin kr - kr \cos kr}{k^3 r^3} \right) \qquad (22)$$

It is more useful to express $\sigma^2(r)$ in the following form

$$\sigma^2(r) = \int \frac{dk}{k} \left(\frac{k^3 P(k)}{2\pi^2} \right) |W(k, r)|^2 = \int \frac{dk}{k} \Delta^2(k) |W(k, r)|^2 \qquad (23)$$

Press-Schecter mass function

If we consider that the initial density field is Gaussian then the fraction of mass $F(M)$ in the collapsed objects with mass greater than M can be identified with the fraction of the initial volume for which $\delta > \delta_c$.

$$F(M) = \int_{\delta_c}^{\infty} P(\delta, r) d\delta = \text{Erfc}\left(\frac{\nu}{\sqrt{2}}\right) \tag{24}$$

$$f(M)dM = \frac{\partial F(M)}{\partial M} = \sqrt{\frac{2}{\pi}} \left|\frac{dln\sigma}{dM}\right| \nu \exp(-\nu^2/2) dM \tag{25}$$

and comoving number density of objects in mass range $[M, M + dM]$ is

$$N(M)dM = \frac{\rho}{M} \times f(M)dM = \sqrt{\frac{2}{\pi}} \frac{\rho}{M^2} \left|\frac{dln\sigma}{dlnM}\right| \nu \exp(-\nu^2/2) dM \tag{26}$$

where $\nu = \delta_c/\sigma$

[Press & Schechter (1974)]

Mode coupling in Non-linear gravitational clustering

- Structure formation in a cold dark matter dominated universe takes place hierarchically. In this situation it becomes relevant to ask:

What role perturbations at small scales (substructure) play in the collapse of perturbations at larger scales ? [Bagla et al. (2005); Bagla & Prasad (2009)]

- It is well knows that there are strong effects of perturbations at large scales on the growth of perturbations at small scales. In cosmological N-body simulations perturbations at scales larger than the size of simulation volume are ignored.

How the size of simulation volume affect various physical quantities in N-body simulations ? [Bagla & Prasad (2006); Prasad (2007); Bagla et al. (2009)]

1. Role of substructure

Name	Method	α	Plane wave	IC
PM_00L	PM	0.0	Yes	Grid
T_00L	TreePM	0.0	Yes	Perturbed grid
T_05L	TreePM	0.5	Yes	Grid
T_10L	TreePM	1.0	Yes	Grid
T_20L	TreePM	2.0	Yes	Grid
T_40L	TreePM	4.0	Yes	Grid
T_10P	TreePM	1.0	Yes	Perturbed grid
T_40P	TreePM	4.0	Yes	Perturbed grid
T_05	TreePM	0.5	No	Grid
T_10	TreePM	1.0	No	Grid
T_20	TreePM	2.0	No	Grid
T_40	TreePM	4.0	No	Grid

Table: Cosmological simulations with power at two scales: large scale (plane wave) and small scales (power non-zero only for a narrow range on scales isotropic and anisotropic). We found that the presence of isotropic power speed-up the collapse of plane wave [Bagla et al. (2005)].

A. Planar Collapse

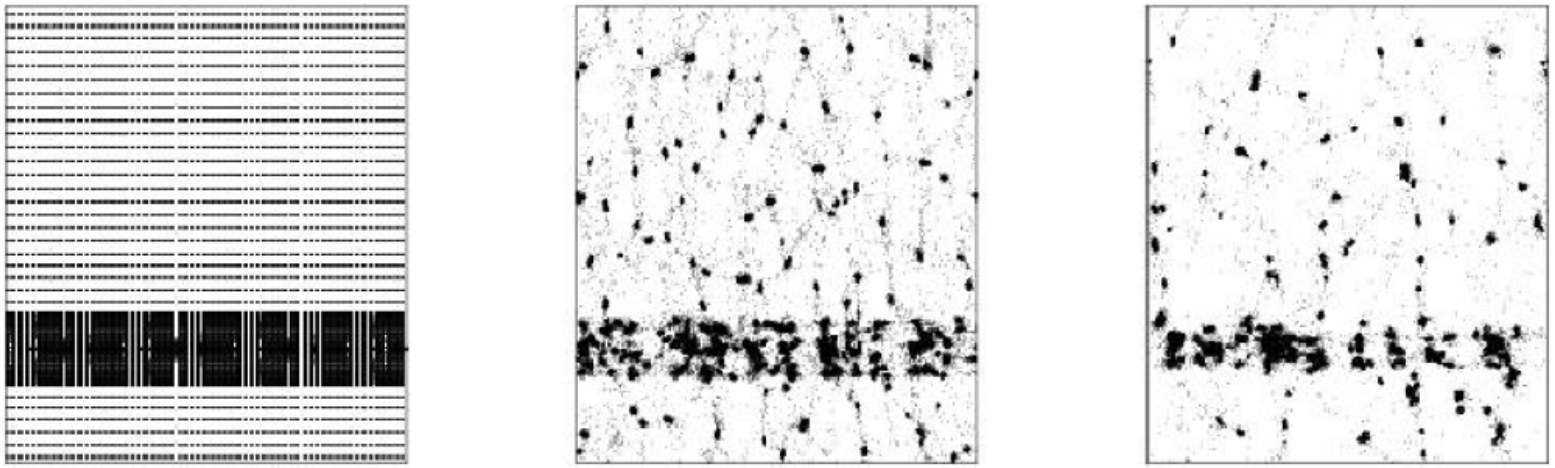

Figure 2.3: The left, middle and right panels in this figure show the slices parallel to the x-z plane at $a = 2$ for simulation T_00L, T_10L and T_40L respectively. Collapse of the plane wave along the vertical direction (z-axis) leads to formation of the pancake. From this figure we can see that the thickness of the pancake decreases when we increase the amount of substructure (when we go from left to right).

[Bagla et al. (2005)]

Planar Collapse

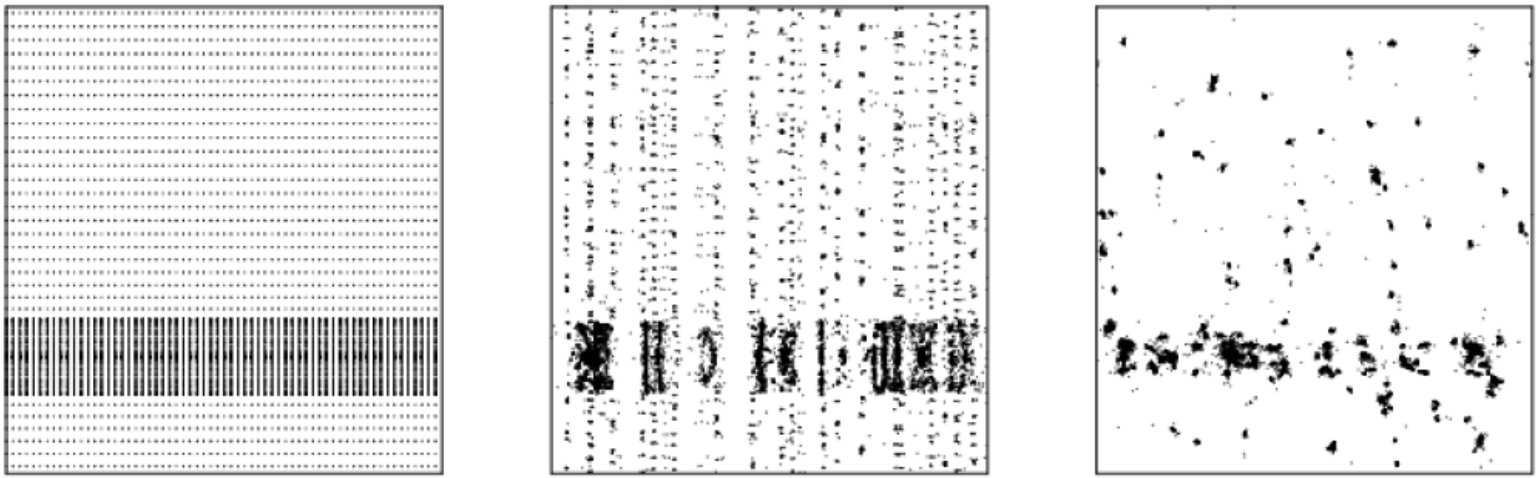

Figure 2.5: The left, middle and right panels in this figure show the slices parallel to the x-z plane at $a = 2$ for simulations PM_00L, T_40P and T_40L respectively. This visual comparison shows that the pancake is thinner in T_40L as compared to T_40P. Indeed, the thickness of pancake in T_40P and PM_00L is very similar.

[Bagla et al. (2005)]

B. Features in Power spectrum

Models

$$P(k) = \begin{cases} Ak^{-1}, & \text{for Model I} \\ Ak^{-1}e^{-\frac{k^2}{2k_c^2}}, & \text{for Model II} \\ Ak^{-1} + A\alpha k_c^{-1} e^{\frac{(k-k_c)}{2\sigma_k^2}} & \text{for Model III} \end{cases} \quad (27)$$

Parameters

$\sigma_k = 2\pi/L_{box}$, $k_c = 4k_f = 4(2\pi/L_{bpx})$, $\alpha = 4$
$r_{nl}(a = 1) = 12$, $N_{part} = 200^3$, $L_{box} = 200$

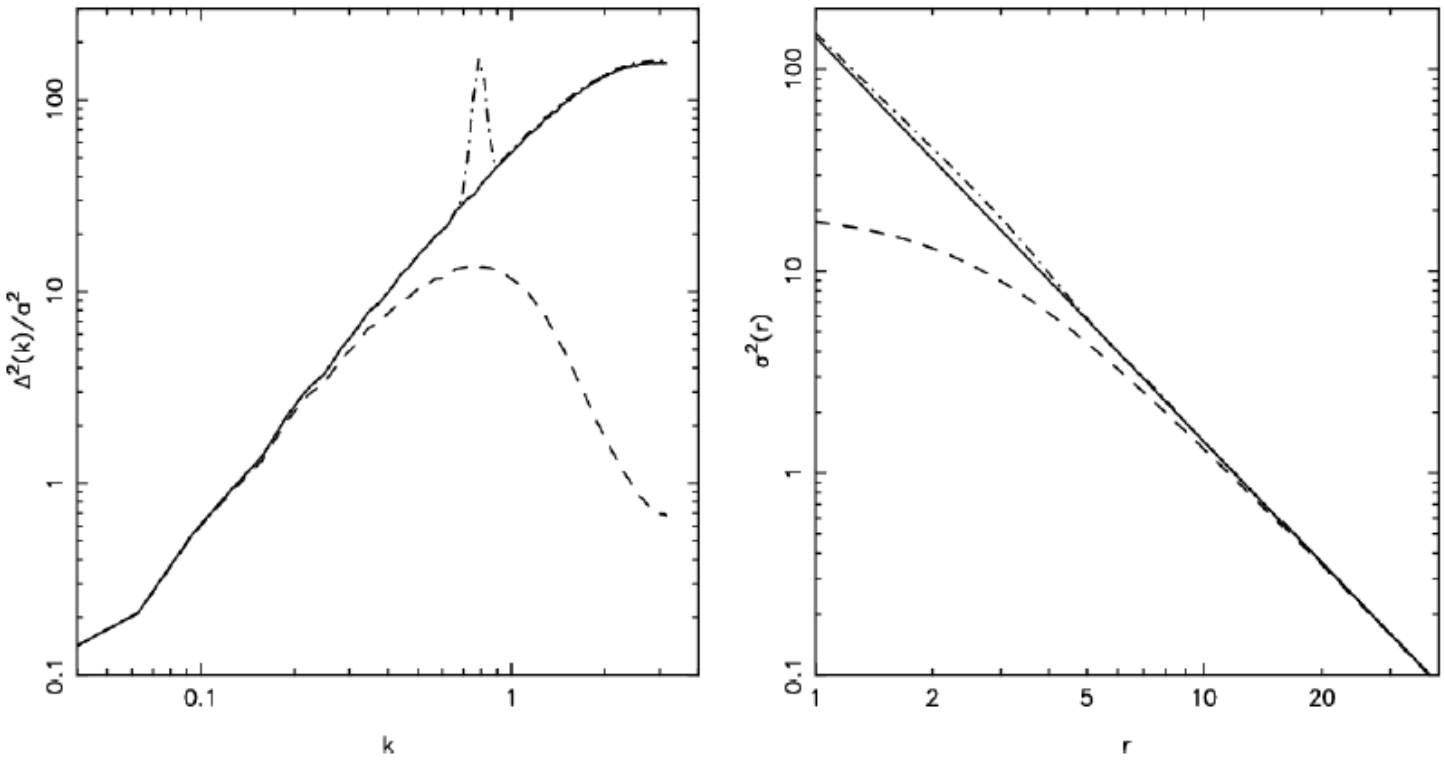

Figure 3.1: The left and right panels in this figure show the linearly extrapolated power spectrum $\Delta^2(k)$ and variance $\sigma^2(r)$ at the epoch $a = 1$. In both the panels models I, II and III are represented by the solid, dashed and dot-dashed lines respectively.

[Bagla & Prasad (2009)]

Correlation function

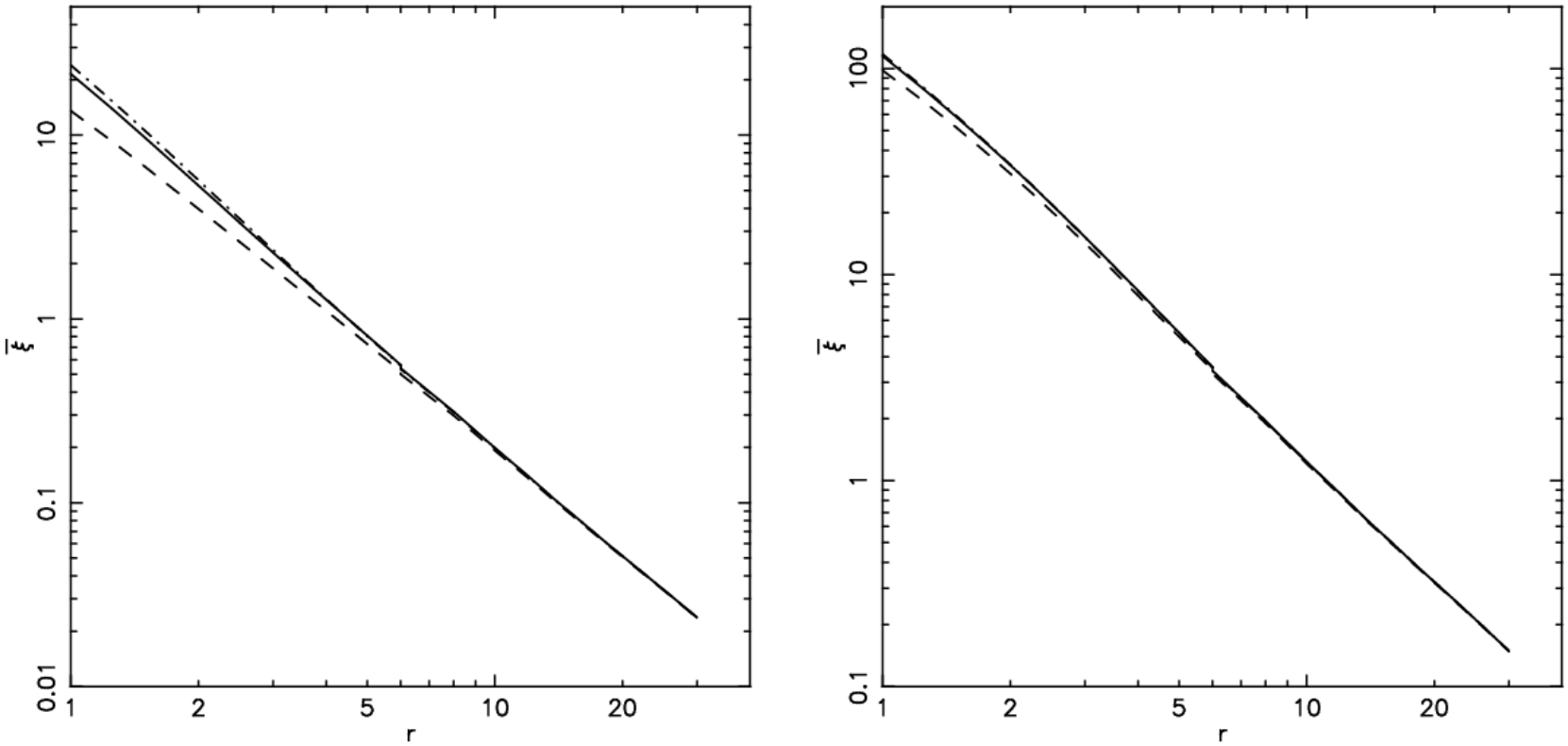

Figure: The left and right panels show the average two point correlation functions for all the models at an early and later epoch respectively.

[Bagla & Prasad (2009)]

Skewness

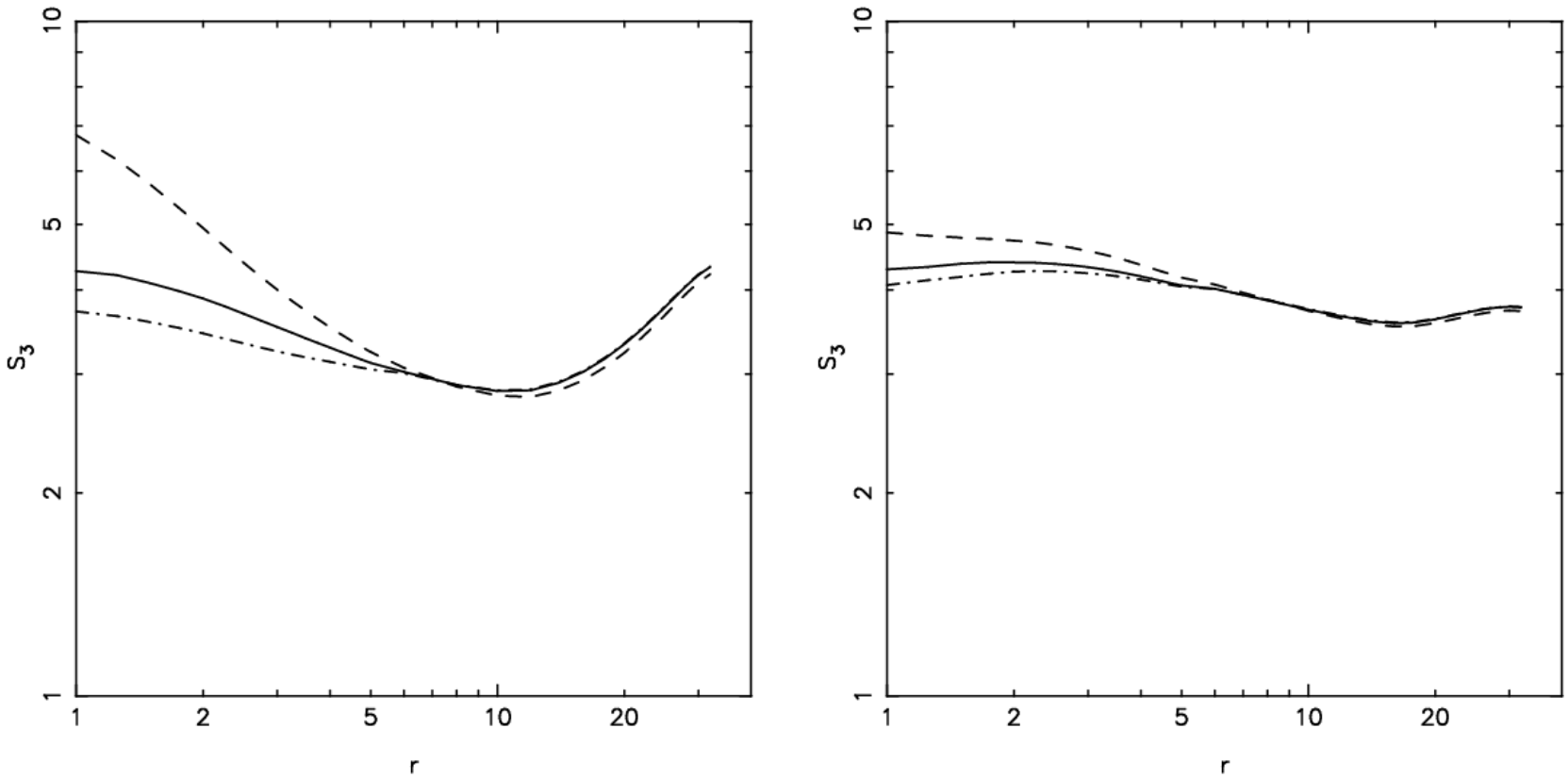

Figure: The left and right panels show the Skewness for all the models at an early and later epoch respectively.

[Bagla & Prasad (2009)]

Number density

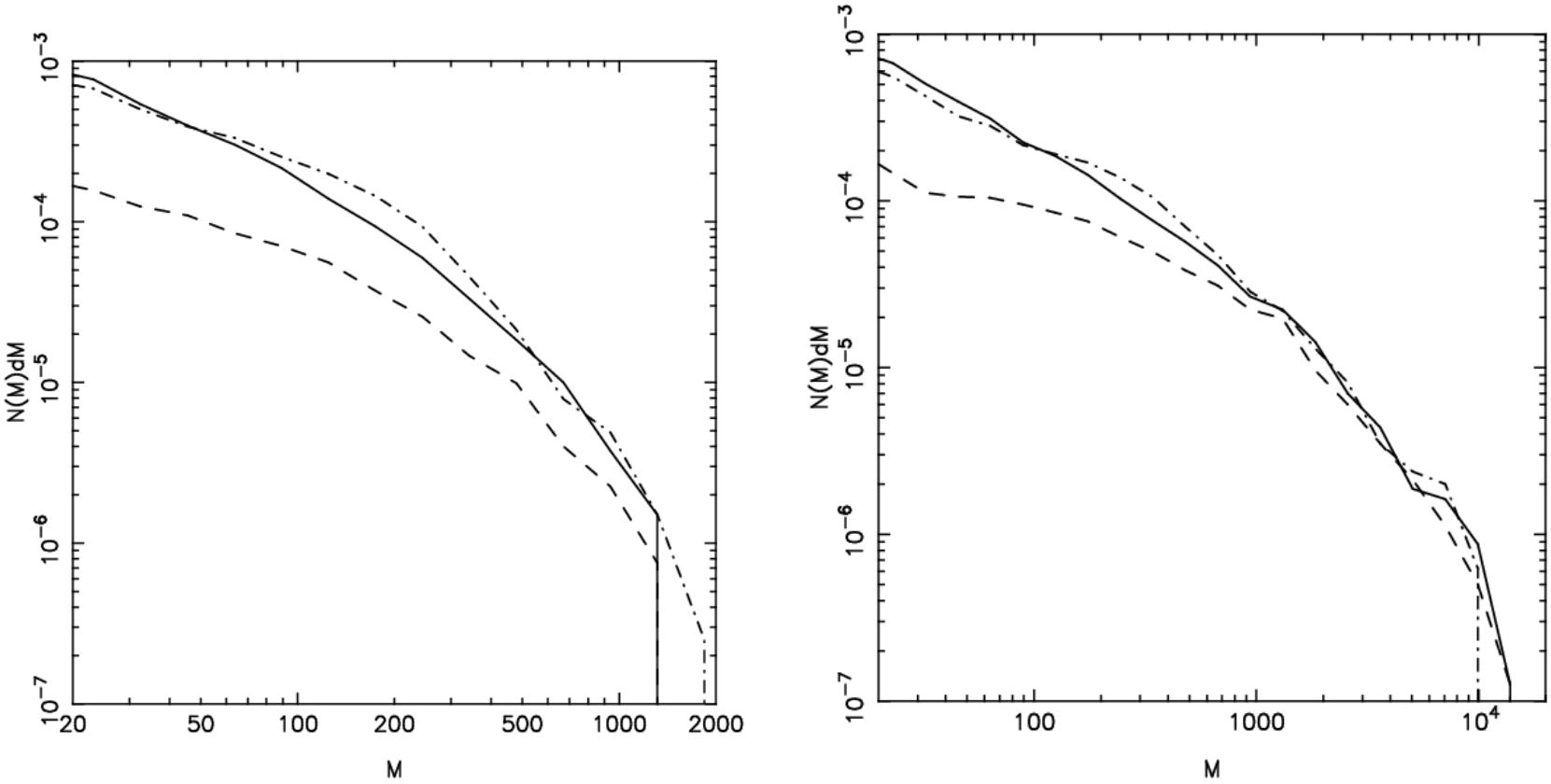

Figure: The left and right panels show the number density of haloes for all the models at an early and later epoch respectively.

[Bagla & Prasad (2009)]

2. Finite volume effects

- In cosmological N-body simulations the initial power spectrum is sampled at discrete points in k space in the range $[2\pi/L_{box}, 2\pi/L_{grid}]$.
- Perturbations $k > 2\pi/L_{box}$ can be ignored since there are no significant effects or perturbations at small scales on large scale. However, that is not the case of $k < 2\pi/L_{box}$ perturbations at scales larger than the simulation volume can affect physical quantities significantly.

[Bagla & Prasad (2006); Prasad (2007); Bagla et al. (2009)]

Our formalism [Bagla & Prasad (2006)]

Mass variance in theory

$$\sigma_0^2(r) = \int_0^\infty \frac{dk}{k} W^2(kr) \quad \text{where} \quad \Delta^2(k) = \frac{k^3 P(k)}{2\pi^2} \tag{28}$$

In simulations

$$\sigma^2(r, L_{box}) = \int_{2\pi/L_{box}}^{2\pi/L_{grid}} \frac{dk}{k} \Delta^2(k) W^2(kr) \tag{29}$$

From the above two equations:

$$\sigma^2(r, L_{box}) = \int_0^\infty \frac{dk}{k} \Delta^2(k) W^2(kr) - \int_0^{2\pi/L_{box}} \frac{dk}{k} \Delta^2(k) W^2(kr) = \sigma_0^2(r) - \sigma_1^2(r) \tag{30}$$

Correction in mass variance

$$\sigma_1^2(r, L_{box}) = \int_0^{2\pi/L_{box}} \frac{dk}{k} \Delta^2(k) W^2(kr)$$

$$\approx C_1 - \frac{1}{5} C_2 r^2 + \frac{3}{175} C_3 r^4 + \mathcal{O}(r^6) \quad (31)$$

where

$$C_n = \int_0^{2\pi/L_{box}} \frac{dk}{k} k^{2(n-1)} \Delta^2(k) \quad (32)$$

Power law model: $P(k) = Ak^n$

$$C_1 = \frac{A}{2\pi^2(n+3)} \left(\frac{2\pi}{L_{box}}\right)^{(n+3)} \quad (33)$$

Correction in Mass function

The Press-Schecter mass function (theory)

$$F(M) = F_0(M) = 2\int_{\delta_c}^{\infty} \frac{1}{\sqrt{2\pi\sigma_0^2(M)}} \exp\left(-\frac{\delta^2}{2\sigma_0^2(M)}\right) d\delta \qquad (34)$$

N-body simulations

$$F(M, L_{box}) = 2\int_{\delta_c}^{\infty} \frac{1}{\sqrt{2\pi\sigma^2(M, L_{box})}} \exp\left(-\frac{\delta^2}{2\sigma^2(M, L_{box})}\right) d\delta \qquad (35)$$

Correction :

$$F_1(M, L_{box}) = F_0 - F = \frac{2}{\sqrt{\pi}} \int_{\frac{\delta_c}{\sigma_0(M)\sqrt{2}}}^{\frac{\delta_c}{\sigma(M,L_{box})\sqrt{2}}} \exp(-x^2)$$

$$\approx \frac{\delta_c}{\sqrt{2\pi}} \frac{\sigma_1^2}{\sigma_0^3} \exp\left(-\frac{\delta_c^2}{2\sigma_0^2}\right) \qquad (36)$$

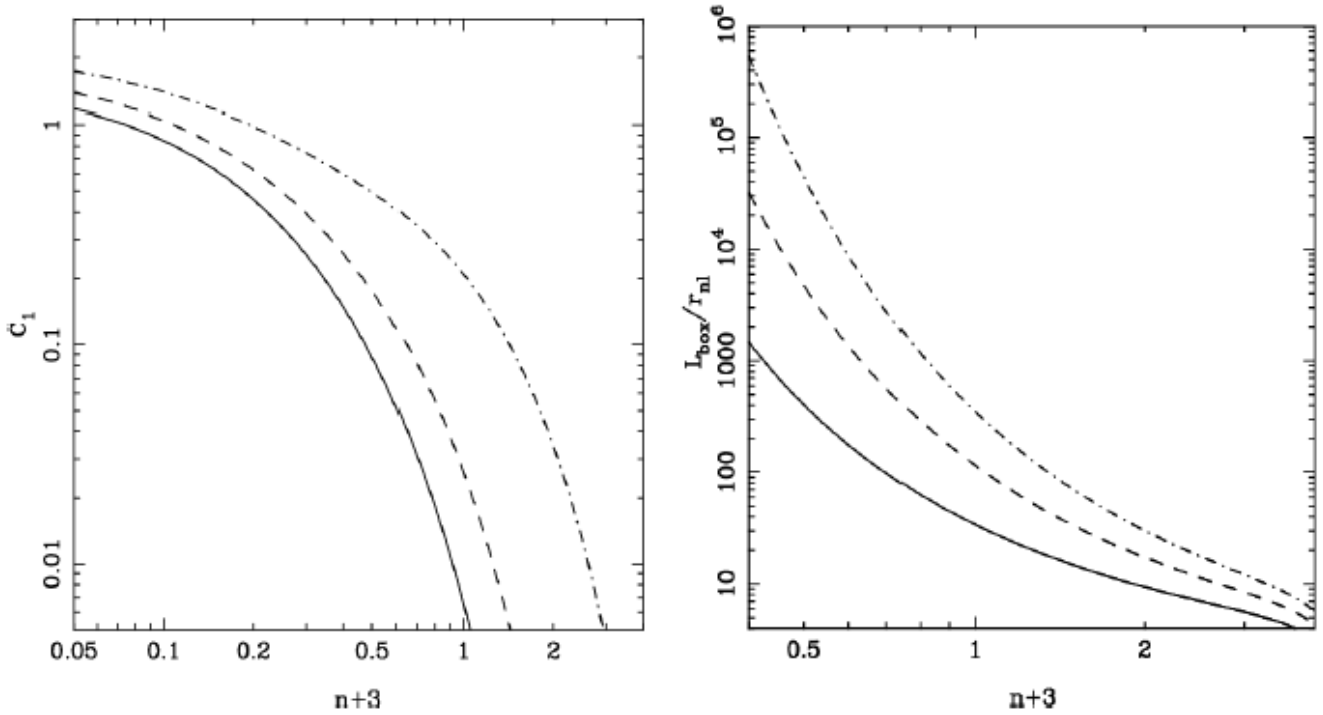

Figure 4.1: The left panel in this figure shows the variation of the leading order correction C_1 with the index of power spectrum n for different values of the size of the simulation box. The curves corresponding to $L_{box}/r_{nl} = 16, 128$ and 512 are represented by the dot-dashed, dashed and solid lines respectively. From this, we notice that the correction term becomes more and more important as n approaches towards -3. The right panel in this figure shows the variation of the size of the simulation box with the index of power spectrum for different values of C_1 (0.01, 0.03, 0.1 from top to bottom)

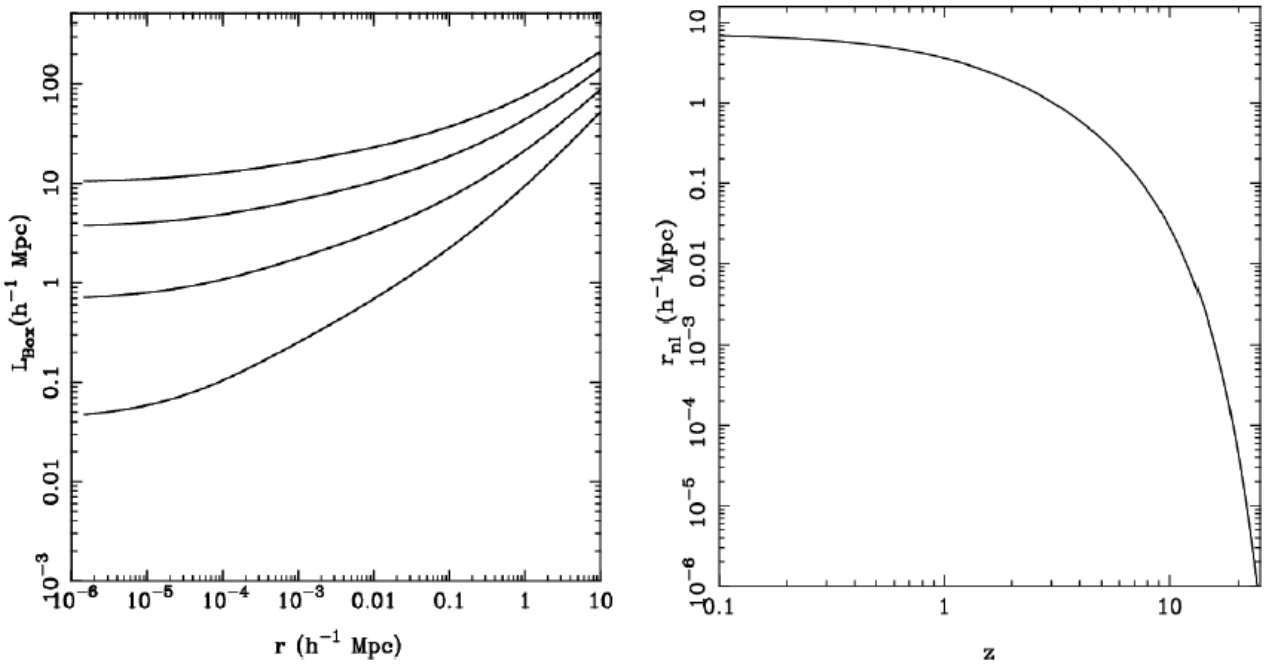

Figure 4.2: The left panel in this figure shows the contours of constant $C_1/\sigma_0^2 = 0.01, 0.03, 0.1$ and 0.3 (from top to bottom) and the right panel shows the variation of the scale of nonlinearity with redshift for the ΛCDM model.

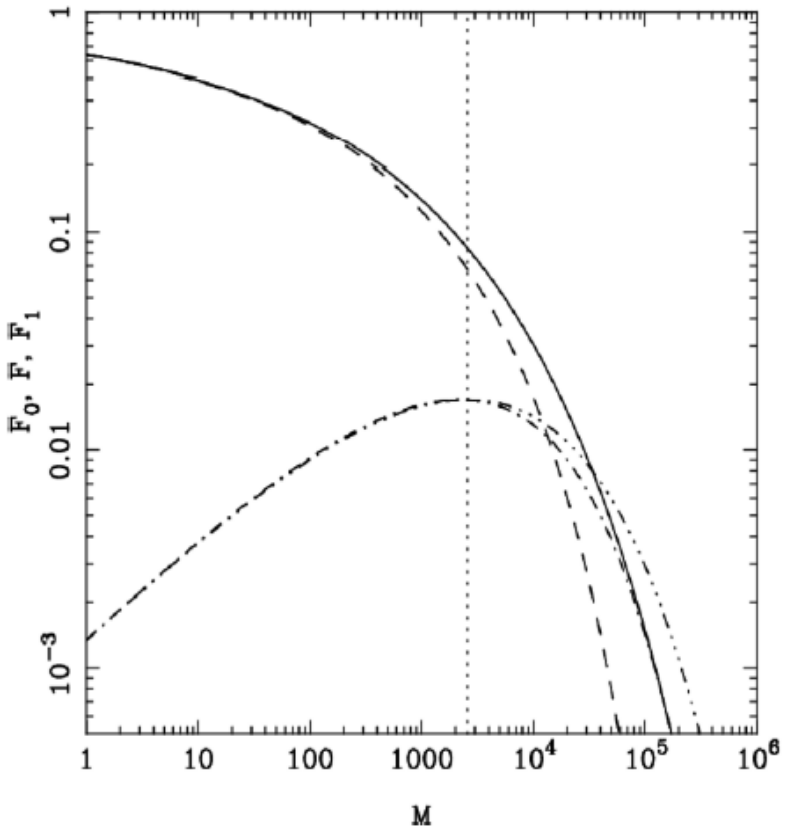

Figure 4.3: This figures shows the exact mass function $F_0(M)$ (solid line) and the mass function $F(M, L_{box})$ (dashed line) which we expect in N-body simulation (dashed line) for a power law model ($n = -2$). The exact and approximate corrections $F_1(M, L_{box})$ in mass function i.e., equation (4.10) and (4.11), are also shown by the dot-dashed and dotted lines respectively. The scale where $\sigma_0 = \delta_c/\sqrt{3}$ is marked with a vertical dotted line which coincides with the maximum of $F_1(M, L_{box})$.

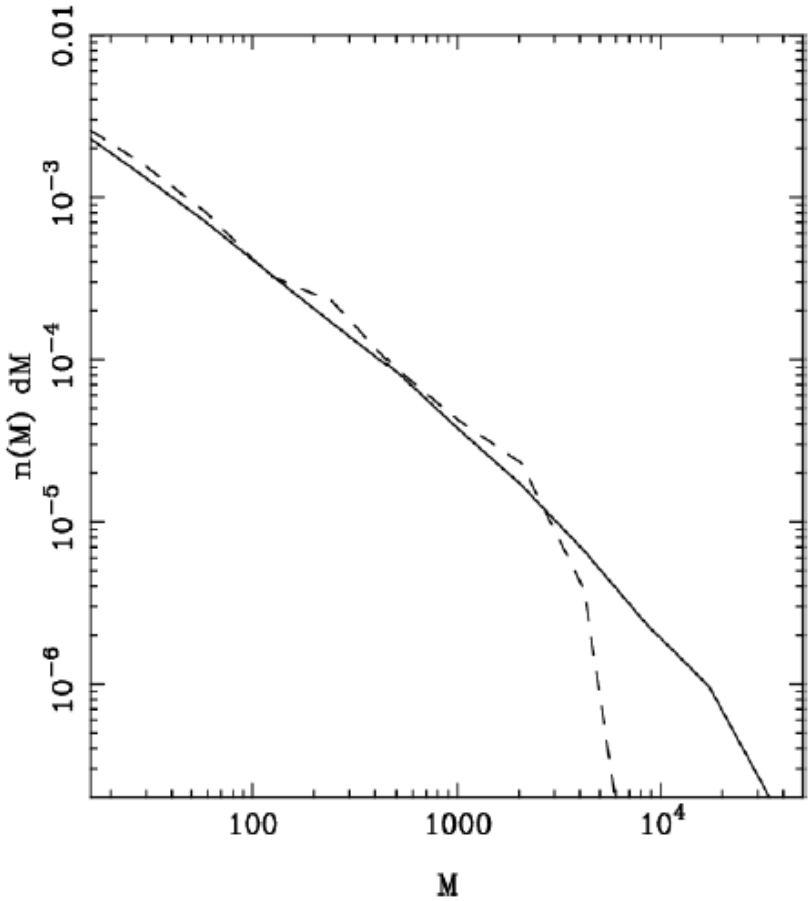

Figure 4.5: This figure shows the comoving number density of haloes $n(M)dM$ in the mass range $M - M + dM$ for the large (solid line) and small (dashed line) simulations (see text). From this figure we observe that the number density of low mass haloes is overestimated in the case of smaller simulations as is expected in this formalism.

Summary & Conclusions

- In the models of structure formation in which cold dark matter is the dominating component, gravitational clustering takes place hierarchically i.e., small structures form first and bigger structures follow later.
- It is important to understand what role substructures play in the collapse of perturbations at larger scales.
- We have found that in most cases the role of structure can be neglected which follows the paradigm that transfer of power in non-linear gravitational clustering is mostly from large to small scales.
- In cosmological N-body simulations perturbations at sub-grid scales are assumed to be zero. Our study can help to understand the effects of pre-initial condition in cosmological N-body simulations.

Summary cont...

- We have developed a prescription for estimating corrections in various physical quantities (related to gravitational clustering) due to the finite size of the simulation box.
- We showed that the amplitude of clustering is underestimated at all scales when the size of simulation volume is reduced.
- We presented explicit expressions for corrections in mass function, multiplicity function, number density and formation and destruction rates of haloes.
- We showed that the correction in mass function is maximum at the scales of non-linearity and it decreases at large as well as small scales.
- We showed that the number density of low mass haloes is overestimated and that of large mass haloes is underestimated when the size of the simulation box is reduced.

Thank You !

References

Aarseth, S. J. 2003, Gravitational N-Body Simulations (Cambridge, UK: Cambridge University Press, November 2003.)

Bagla, J. S. 2002, Journal of Astrophysics and Astronomy, 23, 185

Bagla, J. S., & Padmanabhan, T. 1997, Pramana, 49, 161

Bagla, J. S., & Prasad, J. 2006, Monthly Notices of Royal Aastron. Society, 370, 993

—. 2009, Monthly Notices of Royal Aastron. Society, 393, 607

Bagla, J. S., Prasad, J., & Khandai, N. 2009, Monthly Notices of Royal Aastron. Society, 395, 918

Bagla, J. S., Prasad, J., & Ray, S. 2005, Monthly Notices of Royal Aastron. Society, 360, 194

Bagla, J. S., & Ray, S. 2003, New Astronomy, 8, 665

Barnes, J., & Hut, P. 1986, Nature, 324, 446

Bertschinger, E. 1998, Ann. Rev. Astron. Astrophys., 36, 599

Efstathiou, G., Davis, M., White, S. D. M., & Frenk, C. S. 1985, Astrophical Journal Suppliment, 57, 241

Hockney, R. W., & Eastwood, J. W. 1981, Computer Simulation Using Particles (New York: McGraw-Hill, 1981)

Padmanabhan, T. 1993, Structure Formation in the Universe (Cambridge, UK: Cambridge University Press, June 1993.)

Peebles, P. J. E. 1980, The large-scale structure of the universe (Princeton, N.J., Princeton University Press, 1980. 435 p.)

Prasad, J. 2007, Journal of Astrophysics and Astronomy, 28, 117

Press, W. H., & Schechter, P. 1974, Astrophical Journal, 187, 425

Sellwood, J. A. 1987, Ann. Rev. Astron. Astrophys., 25, 151